Article:
McAlary, L, Harrison, JA, Aquilina, JA et al. (4 more authors) (2020) The trajectory taken by dimeric Cu/Zn superoxide dismutase through the protein unfolding and dissociation landscape is modulated by salt-bridge formation. Analytical Chemistry, 92 (2). pp. 1702-1711. ISSN 0003-2700

https://doi.org/10.1021/acs.analchem.9b01699

The trajectory taken by dimeric Cu/Zn superoxide dismutase through the protein unfolding and dissociation landscape is modulated by salt-bridge formation

Luke McAlary[†⊥], Julian A. Harrison[⊥], J. Andrew Aquilina[†⊥], Steven P. Fitzgerald[‡], Celine Kelso[⊥], Justin L.P. Benesch[§]* & Justin J. Yerbury[†⊥]*

[†]*Illawarra Health and Medical Research Institute, Wollongong, NSW 2522 Australia*

[⊥]*Molecular Horizons and School of Chemistry and Molecular Bioscience, Faculty of Science, Medicine and Health, University of Wollongong, NSW, Australia 2522*

[‡] *Department of Applied Mathematics, University of Leeds, Leeds, LS2 9JT, UK*

[§]*Department of Chemistry, Physical and Theoretical Chemistry Department, University of Oxford, Oxford, OX1 3QZ, UK*

*Address correspondence to:

Justin L.P. Benesch: justin.benesch@chem.ox.ac.uk (+44 0 186-528-5420)

Justin J. Yerbury: jyerbury@uow.edu.au (+61 2 42-981-534)

TOC Illustration

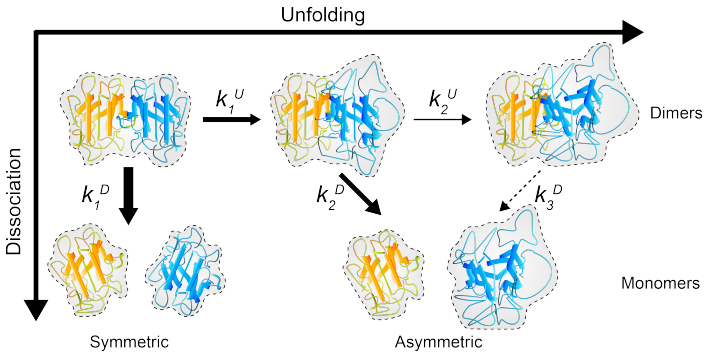

Abstract

Native mass spectrometry (MS) is a powerful means for studying macromolecular protein assemblies, including accessing activated states. However, much remains to be understood about what governs which regions of the protein (un)folding funnel are explored by activation of protein ions in vacuum. Here we examine the trajectory that Cu/Zn superoxide dismutase (SOD1) dimers take over the unfolding and dissociation free energy landscape in vacuum. We examined wild-type SOD1 and six disease-related point-mutants by using tandem MS and ion-mobility MS as a function of collisional activation. For six of the seven SOD1 variants, increasing activation prompted dimers to transition through two unfolding events and dissociate symmetrically into monomers with (as near as possible) equal charges. The exception was G37R, which proceeded only through the first unfolding transition, and displayed a much higher abundance of asymmetric products. Supported by the observation that ejected asymmetric G37R monomers were more compact than symmetric G37R ones, we localised this effect to the formation of a gas-phase salt-bridge in the first activated conformation. To examine the data quantitatively, we applied Arrhenius-type analysis to estimate the barriers on the corresponding free energy landscape. This reveals a heightening of the barrier to unfolding in G37R >5 $kJmol^{-1}$ over the other variants, consistent with expectations for the strength of a salt-bridge. Our work demonstrates weaknesses in the simple general framework for understanding protein complex dissociation in vacuum, and highlights the importance of individual residues, their local environment, and specific interactions in governing product formation.

Introduction

Native mass spectrometry (MS) can be used to reveal attributes of protein assemblies such as oligomeric distribution, topology, and dynamics[1-5]. A key component of this approach is tandem mass spectrometry (MS/MS), in which ion populations within discrete *m/z* (mass-to-charge ratio) regions are isolated and dissociated to provide insight into their underlying composition. This is typically achieved using collision-induced dissociation (CID), where charged complexes are subject to increasingly energetic encounters with a bath gas[6]. Activation results in decomposition of the complex, typically via the loss of monomeric subunits. Dissociation of a complex is considered "asymmetric" when the average partitioning of charge between products is unequal with respect to their mass (e.g. $\text{dimer}^{z+} \rightarrow \text{monomer}^{>(z/2)+} + \text{monomer}^{<(z/2)+}$). This results in products with charge state distributions centred on different *m/z* ratios. By contrast, dissociation is defined as "symmetric" when charge and mass are (on average) apportioned equally over the fragment ions (e.g. $\text{dimer}^{z+} \rightarrow 2\ \text{monomer}^{(z/2)+}$), leading to a unimodal distribution of charge states.

The disproportionately high charge on one of the products of asymmetric dissociation is traditionally rationalised by its collision-induced unfolding (CIU) during activation, with mobile protons[7-8] migrating[9] to the newly exposed, and evolving, surface to maintain (in broad terms) a uniform surface charge-density[10-13]. An alternative model is that the asymmetric partitioning of charge arises from the heterolysis of salt bridges – either already present in solution or freshly formed in the gas-phase – in a manner that enhances the charge on the leaving subunit[14]. These two models, therefore, differ considerably in explaining variations in charge partitioning, either via differing extents of protein unfolding, or number of heterolytic salt-bridge cleavages.

Ion mobility-mass spectrometry (IM-MS) has allowed the measurement of complexes during activation, returning collision cross-sections (CCSs) consistent with unfolding of a constituent

subunit[15]. The extent and pathway of unfolding prior to dissociation is however variable, and depends on the protein complex, the experimental conditions, and charge state[16-18]. For instance, asymmetric partitioning of charge can also occur with little or no unfolding, as has been observed for low charge states of the tetrameric proteins C-reactive protein and concanavalin-A[18], and transthyretin[16], undergoing CID. These studies demonstrate how the relationship between charging and unfolding is not simple, and processes including the formation of new bonds within the proteins and cleavage of interfacial salt bridges may be operative[14].

Given this variability, rather than being independent and sequential processes, structural distortion (encompassing both unfolding and new bond formation) and dissociation are better considered as two dimensions of the conformational space accessible to a protein complex during gas-phase activation[19]. The trajectory ions take over this gas-phase distortion-dissociation energy surface has been exploited to characterise protein and protein-ligand complexes[20]. However, to advance the diagnostic utility of this approach, we require a deeper understanding of the mechanistic determinants of the pathway taken[21]. Here we have addressed this deficiency by examining quantitatively the behaviour of wild-type (WT) and mutant forms of Cu/Zn superoxide dismutase (SOD1), upon collisional activation.

SOD1 is a 32 kDa homodimeric enzyme that converts superoxide to either oxygen or hydrogen peroxide[22]. Each monomer contains a catalytically active copper atom, a zinc atom, and an intra-monomer disulfide bond (Fig. 1A). Amyotrophic lateral sclerosis-associated mutations are found throughout the SOD1 sequence and result in variations in protein stability, including dimer affinity[23-25], leading to an increased propensity for misfolding and aggregation[26]. We have exploited this system, building on work showing the susceptibility of bovine SOD1 to activation in the gas-phase[27] to interrogate the relationship between unfolding and the symmetry of

dissociation upon collisional activation. We were able to characterise in detail the unfolding and dissociation pathways of the SOD1 dimer and develop an analysis framework that provides a quantitative interpretation of the data. Our approach revealed that dimers of the G37R mutant of SOD1 have a higher propensity to dissociate asymmetrically yet, surprisingly, the more highly charged monomers were more compact for this mutant. G37R is also unusual in that it proceeds towards dissociation through only one of the two unfolded conformers seen for the wild-type (and other variants). We are able to rationalise these observations through the formation of a new salt-bridge during unfolding that remodels the energy landscape relative to the wild-type protein. Together, these results further our understanding of gas-phase protein dynamics and provide insight on the influence of charge and electrostatic interactions on the free energy landscape they explore.

Experimental section

Materials. All solutions were prepared using Milli-Q ultra-purified water obtained from a Millipore purification system (Massachusetts, USA). All materials were of analytical grade. Tryptone, Tris-base, DTT, β-Mercaptoethanol, bromophenol blue, brilliant blue G, ammonium persulphate, SDS, ampicillin sodium salt, and IPTG were from Amresco (Ohio, USA). NaCl, ammonium sulphate, agar, acetonitrile, Tris-HCl, EDTA, ammonium acetate, and RNase were from Sigma-Aldrich (Missouri, USA). DNase was from Roche Diagnostics (NSW, Australia). Carbenicillin was from Carbenicillin Direct (UK). Copper sulphate pentahydrate was from Ace Chemical Company (SA, Australia). Zinc sulphate heptahydrate was from Hopkin and Williams LTD (Birmingham, UK). Formic acid and acetic acid were from Univar (NSW, Australia). Methanol was from Ajax Finechem (NSW, Australia). Gold coated borosilicate capillaries were made in house using borosilicate capillaries from Harvard Apparatus (Massachusetts, USA) using a P-97 Flaming/Brown micropipette puller (Sutter Instruments, USA)

Expression and purification of recombinant human SOD1. Bacterial expression plasmids encoding SOD1 WT, A4V, G37R and G93A were a kind gift from Professor Mikael Oliveberg (Stockholm University, Sweden). SOD1 mutants H46R, D90A, and V148G were designed in house and generated by Genscript (New Jersey, USA). Protein expression and purification were performed according to previous work[28]. Briefly, SOD1 was co-expressed with the yeast copper chaperone in the presence of copper and zinc ions in chemically competent BL21(DE3) *E. coli*, to promote native folding of SOD1 protein. *E. coli* were lysed using an Emulsiflex-C5 (Avestin Inc, Canada). Lysates were subject to heat denaturation at 65 °C and cleared by centrifugation, following which ammonium sulphate precipitations at 60% and 90% (w/v) were performed at 4 °C. The 90% ammonium sulphate precipitated pellet was resuspended and purified using a

combination of gel filtration (Hiload 16/60 Superdex 75 PG, GE USA) and anion exchange chromatography (Hiscreen Capto-Q, GE USA). Pure SOD1 was pooled and flash-frozen with liquid nitrogen before storage at -20 °C.

Sample preparation for Mass Spectrometry. Purified SOD1 samples were desalted and buffer exchanged into 200 mM NH_4OAc (pH 6.8), using gel-filtration chromatography (Superdex 75 10/300 GL, GE USA). The SOD1 concentration from collected fractions was determined using a bicinchoninic acid assay. Samples were diluted to 10 μM (monomer) using 200 mM NH_4OAc (pH 6.8) prior to mass spectrometry. The WT•G37R heterodimer samples were generated by mixing equal parts WT homodimer and G37R homodimer, both in 200 mM NH_4OAc (pH 6.8), together and incubating overnight at 37 ºC so that subunit exchange would occur. Paradoxin was purified from inland taipan (*oxyuranus microlepidotus*) lyophilized whole venom by resuspending lyophilized protein into 200 mM NH_4OAc prior to gel-filtration chromatography (Superdex 200 10/300 GL, GE USA)[29]. Paradoxin was diluted to 10 μM prior to nanoelectrospray ionization mass spectrometry.

Mass Spectrometry. All MS experiments were performed using a SYNAPT G1 HDMS (Waters, UK) in positive ion mode with a nano-electrospray ionisation source, along the lines described previously[30]. Instrument parameters were: capillary 1.52 kV, sample cone 70 V, accelerating potential into the "transfer" collision cell 4 V, accelerating potential into the "trap" collision cell 6-100 V, ion transfer stage pressure 0.42 mbar, ToF analyser pressure 2.38×10^{-6} mbar, backing pressure 4.0 mbar. The collision gas was Argon. For tandem MS experiments, a peak window centred on ~2900 *m/z* was used, and the accelerating potential into the trap collision cell was increased from 6 to 100 V in 5-V increments. For IM-MS, settings were similar to those described previously[15], with the exception of the instrument parameters listed above. No mobility selection

was used in the experiments or data extraction. All spectra were externally calibrated using a solution of caesium iodide (10 mg/ml in 50% n-propanol). Spectra were processed and analysed using Masslynx 4.1 and Driftscope 2.1 software (Waters, UK). CIU fingerprints were generated and analysed using CIUSuite[31].

CCS measurement of SOD1 ions. CCS values of SOD1 ions in the gas phase were measured and calculated according to a previously protocol[32]. Briefly, the CCS calibrants were subunits (β and γ) and trimer of the phospholipase A_2 protein, Paradoxin (PDx), sourced from Taipan snake venom (Venom Supplies PTY LTD, Tanunda Australia) which were sprayed under similar conditions with the exception of the PDx (10 V Trap collision energy and 10 V Transfer collision energy). Arrival times of the calibrant ions were measured at wave heights of 10.5, 11.0, and 11.5 V. SOD1 WT was sprayed under different accelerating voltages into the Trap voltages (6, 40, 80 V), where a selection window of ~2900 *m/z* was applied for the 40 and 80 V experiments to measure the CCS values of D^{11+} upon activation (i.e. D_2 and D_3), as well as the ejected monomers. We used two previously published methods[33-34] to analyse calibration curves and calculate the CCS values of SOD1 WT protein from the measured arrival times. Experimental CCS values were compared to *in silico* predicted CCS values from several SOD1 x-ray crystal structures (monomer: 2XJK[35], dimer: 2C9V/2C9U[36]) using IMPACT[37] with an atomic radius of 1.68 for the gas probe[38].

Analysis of dissociation and unfolding kinetics. A model describing the competing dimer unfolding and dissociation pathways was generated from assessment of both CID and CIU data of the dimer 11+ charge state (D^{11+}). The sum of the intensities of the 7+ and 4+ monomer charge states was defined as the abundance of the asymmetric products (M_A), with the 6+ and 5+ that of the symmetric products (M_S). This definition ignores the possibility of some "mixing" of dissociation channels, a necessary simplification but one that could be a potential source of error

in our model. The three different dimer conformers were denoted D_1, D_2 and D_3 in order of increasing collision cross-section area (CCS), as revealed by the CIU data. We considered the unfolding transition from D_1 to D_2 to be characterised by the rate constant k_1^U, D_2 to D_3 by k_2^U, the dissociation of D_1 into M_S by k_1^D, and D_2 and D_3 into M_A by k_2^D and as k_3^D, respectively. Rate equations were written for each transition, in terms of the above rate constants and abundances of each of the five states D_1, D_2, D_3, M_A, and M_S, and solved analytically as described in the Supporting Information. Abundances of the species were determined by extracting the signal belonging to each state, and measuring the area under the curve for each state. Arrhenius-type analysis was performed by converting the experimental collision voltages into effective temperatures as previously described[39].

Results

SOD1 dissociates into monomers with differing charge and size

To examine in detail the dissociation of a homodimeric protein in vacuum, we chose to exploit the system afforded by SOD1, both the WT protein and six disease-related single-point-mutants (A4V, G37R, H46R, D90A, G93A and V148G) (Fig. 1A). We first obtained native mass spectra of WT SOD1 at a range of activation potentials into a collision cell containing a low pressure of argon (Fig. 1B). In line with previous data[24, 27], the SOD1 dimer ionized primarily in 10+ and 11+ charge states, with minor populations of 9+ and 12+ (hereon designated X^{z+}, where X denotes the oligomeric state and *z* the integer charge) (SFig. 1). When the SOD1 dimers underwent CID (performed in the "trap" collision cell of a Synapt G1 instrument, throughout this work), the resulting monomer charge states M^{5+} and M^{6+} overlapped with those of the dimer, D^{10+} and D^{12+} respectively. To overcome any ambiguity this might cause, we employed MS/MS to interrogate selectively the D^{11+} ions (~2900 *m/z*, no overlap) and enabling us to quantify unambiguously their decay, and the concomitant evolution of monomers with charge states from 4+ to 7+ (Fig. 1B).

To assess the folding state of SOD1 in the gas phase quantitatively, we determined the CCS of the D^{11+} and each of the monomer charge states individually by means of IM-MS and calibration using known standards. At the lowest accelerating potential into the collision cell (6 V), we obtained a value of 27.3 nm^2 for the D^{11+}, slightly lower than the 29.2 nm^2 estimated from the crystal structure (STable 2). This is consistent with a slight compaction of the structure, arising presumably from the collapse of flexible loops and sidechains protruding from the surface and the formation of new interactions enabled in the absence of solvent[40-42]. At 80 V, all four monomer charge states were detectable, allowing us to determine their CCSs. We found that they ranged from 19.0 nm^2 (M^{7+}) to 13.7 nm^2 (M^{4+}), while that of the monomer excised from the crystal structure was 17.7 nm^2.

This reveals that relative to the native structure M^{7+} is somewhat unfolded (despite the intra-monomer disulphide bond), while the other charge states (notwithstanding the calibration errors associated with low charge state CID products[43]) are slightly compacted. As such, dissociation of SOD1 results in a set of monomeric products that differ both in the charge they carry, and their measured CCS.

SOD1 undergoes both symmetric and asymmetric dissociation into monomers

Considering charge conservation, the dissociation of D^{11+} occurs via two routes, resulting in either M^{5+} or M^{6+} (symmetric dissociation, as non-integer charge states are impossible, M_S), or M^{4+} and M^{7+} (asymmetric, M_A). As the activation potential was increased, we observed a decrease in the relative abundance of D^{11+} (Fig. 1B). The resulting breakdown curve is visibly biphasic, with each phase corresponding to exponential decay of the dimer, suggestive of two CID pathways (Fig. 1C). The first phase is operative in the range 6-70 V and the second over 70-100 V (Fig. 1C, inset). Using stepwise regression, we found no statistical justification for a higher order (i.e. triphasic) fit. Examination of the spectra at low activation potential (20 V) showed no noticeable signal for the asymmetric products (SFig. 2). We therefore calculated the ratio of asymmetric versus symmetric products (M_A/M_S), and found that it increased as a function of activation (Fig. 1D). These data reveal that first of the two phases aligns to symmetric dissociation, and the second to the asymmetric pathway.

We next performed analogous experiments to examine the CID behaviour of the SOD1 mutants. All six assembled into dimers, and we were able to obtain breakdown curves for the D^{11+} ions in each case. The data for the mutants was broadly similar to the WT protein (Fig. 1C), however dissociation of G37R resulted in a dramatically higher abundance of the asymmetric products

compared to the other proteins (Fig. 1D and inset, SFig. 3A). This suggests a remodelling by this particular mutation of the energy landscape leading to dissociation.

Collisional activation results in three distinct conformers of the SOD1 dimer

Having examined the dissociation of D^{11+} ions, we turned to examining their unfolding behaviour by performing CIU on both the WT and mutant D^{11+} ions (Fig. 2A, left row). We observed that with increasing activation the D^{11+} ion transitioned from its native conformation (D_1, 27.3 nm^2) to others (D_2, 31.1 nm^2; and D_3, 32.8 nm^2) appearing at successively later arrival times, consistent with global unfolding of tertiary structure prior to dissociation (STable 2). From this data we were able to calculate the root-mean-square deviation (RMSD) of the CIU data between each mutant and the WT (Fig. 2A, right). We observed low deviations between replicates of the same protein mutant (SFig. 4A and B) and determined significant differences in the CIU of the dimer of mutants to WT by comparing the internal RMSDs (replicates of a single mutant) against RMSDs of mutant *vs* WT. This reveals that only G37R had a significantly altered unfolding profile compared to WT (RMSD = 19.20 ± 0.38%, $p < 0.0001$ SFig. 4B), in line with first visual impressions (Fig. 2A). Plotting the relative abundances of each conformer as a function of activation showed the origin of this difference lies in the transition between D_2 and D_3, the latter state populated only sparingly in the case of G37R (Fig. 2B and SFig. 4C).

The WT•G37R heterodimer unfolds intermediate to both heterodimers but does not dissociate more asymmetrically

In response to the dramatic differences in CIU and CID behaviour observed between G37R and the other proteins, we generated a heterodimer by mixing equimolar amounts of WT and G37R and incubating them at 37 ºC overnight (SFig. 3B). We first assessed the dissociation of this WT•G37R heterodimer (and concomitant evolution of monomers), and found that its breakdown curve was similar to that of both WT and G37R homodimers (Fig. 3A). Notably, the M_A/M_S ratio for the heterodimer was similar to that for WT, and distinctly different to that for G37R (Fig. 3B). In principle, the dissociation of the WT•G37R heterodimer could proceed through four different pathways resulting in different monomer pairs, depending on the amount of charge partitioned to each type of subunit. For both symmetric (either WT^{6+} and $G37R^{5+}$, or WT^{5+} and $G37R^{6+}$) and asymmetric (either WT^{7+} and $G37R^{4+}$, or $G37R^{7+}$ and WT^{4+}) pairs we observed that there was no preferential charge enrichment on either subunit (Fig. 3C).

We next examined the unfolding of the heterodimer D^{11+} ion, and found that it proceeded through the same conformational states as the other proteins. However, we observed that D_2 and D_3, after the initial unfolding of D_1, are populated to approximately equal amounts (Fig. 3D). Comparing the CIU data to that for WT and G37R (Fig. 3E and F) revealed significant differences in CIU in each case for their RMSDs (10 and 14%, respectively) reflecting that the unfolding of the heterodimer lies intermediate to the homodimers. These data indicate that the heterodimer can dissociate via the unfolding of either one of the two subunits.

The dissociated 7+ G37R monomer is more compact than the wild-type and other mutants

We hypothesised that clues as to the anomalous behaviour of the G37R variant – its high tendency for asymmetric dissociation, and its low population of D_3 – might be found in examining the conformation of the monomeric products. We therefore measured the arrival times of the

dissociated monomers (M^{4+}, M^{5+}, M^{6+}, and M^{7+}) from all homodimers, across activation energies where they were abundant, and compared the CIU fingerprints of the mutants to that of the WT. Assessment of the dissociated M^{4+}, M^{5+} and M^{6+} conformers yielded minimal difference between all mutant arrival times compared to WT, and within replicates of each respective monomer (SFig. 4A-C). However, a substantial difference was observed when comparing WT and G37R M^{7+} ions, which were 11.3 ms and 10.5 ms respectively (Fig. 4A), indicating that latter was more compact after its dissociation from the D^{11+} parent ion. While this corresponds to an approximately ~4% smaller CCS than the WT^{7+}, notably $G37R^{7+}$ remains larger than the lower charge-state monomers. This compaction was also apparent in G37R M^{7+} dissociated from the WT•G37R heterodimer, suggesting that this phenomenon is a property of the subunit, not the dimer. Again, we compared the RMSDs of mutants *vs* WT to the RMSDs of internal replicates to determine significance (Fig. 4B). The difference in M^{7+} CCS compared to the internal deviation was significantly greater for the M^{7+} ions from the G37R homodimer (12.06 ± 1.81 %, $p < 0.001$) and for the G37R M^{7+} ion from the heterodimer (8.79 ± 2.90 %, $p< 0.001$) showing that this difference was only apparent in the G37R M^{7+} conformer.

Kinetic modelling of dissociation and unfolding determines thermal and athermal processes

Having established the dissociation and unfolding profiles of the SOD1 dimer, we attempted to gain a more quantitative insight into the free energy landscape underpinning these processes to enable comparison between the mutants. We formalised a parsimonious model, as per Occam's razor, based on the key observations of three-state dimer unfolding, with symmetric dissociation being preferred at low activation, and asymmetric at higher potentials (Fig. 5A). We ascribed rate constants k_1^U and k_2^U to the two unfolding steps, and k_1^D, k_2^D, and k_3^D to dissociation from each of

the three dimer conformations D_1, D_2, and D_3, respectively. The resulting five rate equations for five unknown rate constants are fully determined, and could therefore be solved for each protein at each activation potential measured (Supp Info. Section 1.1). Conversion of the activation potentials into effective temperatures[39] allowed us to perform Arrhenius-type analysis for the five different unfolding and dissociation processes. For all proteins, k_1^U and k_1^D displayed thermal, Arrhenius behaviour (corresponding to a simple barrier transition process) over the relevant effective temperature range (STable 1, SFig. 6A and C). However, k_3^D did not do so for any of the proteins (STable 1). This absence of linearity may be due simply to relatively low flux down the relevant channels. This is consistent with dissociation from D_3 being a minor dissociation channel, with it only being populated at the highest potential (Fig. 2A), at which point the majority of dimer dissociation has already occurred (Fig. 1C). Alternatively, it could indicate that a more complex process underlies these transitions which cannot be adequately modelled by a single barrier.

We observed Arrhenius behaviour for k_2^U for all proteins except G37R, and k_2^D for G37R and the heterodimer only (STable 1, SFig. 6B and D). This suggests that the flux to D_3 is atypically low for G37R, with its D_2 conformation preferentially dissociating, rather than unfolding. Notably, the thermal behaviour of both k_2^U and k_2^D for the heterodimer indicates that it proceeds with sufficient flux down both channels, consistent with it containing both WT and G37R subunits. Again, we are not able to rule out that the non-linearity of the Arrhenius plots is due to a more complex process than we are able to model given the constraints of our data. Irrespectively, these insights align with the qualitative impression from inspection of the data, with asymmetric dissociation products being more abundant for G37R than the other proteins (Fig. 1D), at the expense of populating D_3. (Fig. 2A and B).

These consistencies gave us confidence that our model encapsulates the key features of the data, allowing us to extract effective activation energies (E_a^{eff}) (i.e. barrier heights, for each channel from the Arrhenius plots). This reveals that, in all proteins, the barriers to unfolding ($E_a^{eff}{}_1^U$) and dissociation ($E_a^{eff}{}_1^D$) of D_1 are both approximately 4 kJ/mol (Fig. 5B). The fact that they are similar, is consistent with both processes (D_1 unfolding to D_2, and D_1 dissociating into M_S) being observed. The fate of D_2 varies between G37R and the other proteins. For G37R the barrier for dissociation is quantifiable ($E_a^{eff}{}_2^D$ ~9 kJ/mol) but unfolding is not. For the other homodimers, dissociation is not quantifiable but unfolding is ($E_a^{eff}{}_2^U$ ~4.5 kJ/mol) (Fig. 5B, STable 1). The WT•G37R heterodimer, because it contains both types of subunit, has sufficient flux down each channel and therefore both unfolding and dissociation are measurable and align with the values from the homodimers (Fig. 5B). Since both channels are quantifiable in the heterodimer despite a 5 kJ/mol difference between the barrier height, we can infer that the barrier for unfolding in the G37R must be >5 kJ/mol higher than that for dissociation. As such, our methodology provides a means for quantitative comparison between different proteins, and their respective free energy landscapes.

Discussion

Our detailed interrogation of the CIU and CID of the SOD1 dimer provides us an opportunity to propose a mechanism for these gas-phase processes. First, we considered the striking observation that of the six mutants examined, only G37R behaved significantly differently to the WT. We note that in this case the non-polar glycine in the WT is swapped to an arginine, the sidechain with highest gas-phase basicity and hence readily charged[44]. There are only four arginine residues in a WT monomer, so the consequence of this change is that (in positive-ion electrospray) this site is highly likely to be protonated and thereby available to engage in electrostatic interactions with nearby residues. By contrast, the other mutants either involve the swap of one non-polar sidechain with another (A4V, G93A, V148G), the replacement of an acidic sidechain with a non-polar one (D90A), or only causing a minor increase in gas-phase basicity (H46R)[44]. This highlights the profound impact the presence and location of protonatable sites has on the behaviour of protein ions upon activation in the gas-phase[21].

Next, we considered the origin of the three dimer conformations: the native state (D_1) and the two larger states (D_2 and D_3). One might assign D_2 to (partial) unfolding of one monomer in the dimer, and D_3 the (additional) equivalent unfolding of the other. However, if this were the case, since we can reasonably expect both subunits in the homodimers to behave indistinguishably, we should observe D_2 and D_3 states in all cases. That D_3 is not ubiquitous (it is absent in the G37R homodimer) speaks against this, suggesting instead that the CIU profile we observe is better explained by stepwise unfolding of the same monomer (Fig. 6). While there is a general correlation between the number of unfolding steps and the number of domains in a protein, we note that this is a charge-state dependent phenomenon[17], and that multi-step unfolding of various single-domain

proteins has been reported[45-46], revealing a richness of information in the CIU trajectory beyond domain stoichiometry.

The mutation G37R stabilises the protein versus the second of the two unfolding steps. This suggests that the positively charged arginine participates in an intra-monomer salt-bridge (which necessarily can't be formed by the glycine in the WT). This implies the presence of negatively charged moieties on the net positively charged protein surface, which may seem surprising but has been shown both experimentally and computationally[44, 47], and is evidenced in the formation of salt-bridges as a natural consequence of desolvation [14, 40, 42, 48].

The existence of such an intra-monomer salt-bridge, and the modification of the coulombic repulsion and attraction network, should not make dissociation of the G37R dimer significantly more difficult than the dimer, but would instead modify the free-energy landscape of the individual subunits, altering their gas phase conformation and making them harder to unfold than the WT. This is consistent with our observation of the G37R M^{7+} conformer being more compact following dissociation. Moreover, our kinetic analysis suggested in increase in the unfolding barrier height >5 kJ/mol in G37R, in line with the typical strength of a salt bridge.

There are two potential explanations as to why only the second of the unfolding steps is stabilised by this salt bridge. Either the salt bridge exists in the native state, but the D_1 to D_2 transition results from breakage of contacts elsewhere in the protein. Or, the salt bridge is only formed in D_2, facilitated by the molecular rearrangements in the earlier unfolding event. The former possibility would imply that unfolding happens in one region of the protein before stalling and proceeding in a second location. This is unlikely given the positive-feedback loop of charge migration to newly exposed protein surface with consequent coulombic repulsion of that from the remainder of the complex reinforcing further unfolding[49]. Hence it appears more probable that unfolding starts and

continues in the same region of the protein, with R37 forming a salt bridge on this trajectory that attenuates further unfolding.

We investigated this possibility by examining a high resolution crystal structure of the SOD1 G37R mutant (PDB: 1AZV)[50], and searching for nearby acidic residues both inter- and intra-monomer. We found six that were within 20 Å, but none closer than 12 Å, well above the ~5 Å separation that would be consistent with a salt bridge in solution (SFig 7 and STable 3a,b). This is in line with our reasoning that the R37 does not form a salt bridge in the native state, but rather needs prior local rearrangements in order to do so. Furthermore, given the respective distances between R37 and nearest acidic residues (STable 3a,b), it appears that that the salt bridge formed is more likely to be intra-monomer, thereby attenuating unfolding rather than dissociation.

It is generally thought that bonds that restrict unfolding lead to more symmetric partitioning of charge during dissociation[51-52]. That is not the case for G37R which, despite containing an intra-monomer salt bridge, is more asymmetric and releases a compact 7+ monomer. We rationalise this by considering the interplay between coulombic repulsion and the gas-phase basicity of subunits in defining protonation [53], and suggest that at the threshold of dissociation charge is more likely to partitioned to a R37-containing subunit due to the lower barrier to charge migration. Although the H46R mutation would suggest a similar mechanism, we can explain its WT-like behaviour through noting that not only is the basicity at that site increased by only <6% upon mutation[44]. Furthermore, R46 is buried within the metal-binding region of SOD1 and can potentially take part in charged interactions with the multiple negatively charged residues in the nearby electrostatic loop[54], most likely residue D124 (4.4 Å from R46 in the crystal structure PDB: 3K91[55], SFig 8 and STable 4). These observations suggest the importance of individual residues, their basicities and local

environment, both in defining the charge partitioning of protein complexes during their gas-phase dissociation, and the structure of the products formed.

Conclusions

Native MS has proven useful for interrogating the molecular characteristics of proteins and the interactions they make with other biomolecules. The bulk of the structural information derived from native MS comes from measurement of the protein under conditions that are optimised, insofar as is possible in the vacuum of the mass spectrometer, to assess the native solution state of the protein. However, the exquisite control of ion motion and activation afforded in the mass spectrometer allows higher energy states to be probed selectively[21, 56]. This feasibility is exploited frequently for identification purposes, such as determining which ligands are bound[57], or categorise proteins through their CIU trajectory[58]. However, ascribing transitions in CIU to specific structural events, let alone using them to inform on the fold of the protein itself, remains a frontier challenge.

In this work we have interrogated in detail the structural changes that the SOD1 dimer, and various of its point mutants, undergo upon gas phase activation. Our results have highlighted how both bond breakage and formation pay a role in governing the trajectory taken and the products observed. Our results are thought-provoking in the context of the understanding what governs the partitioning of charge during gas phase dissociation of protein complexes. In polarising terms, two competing models explain charge partitioning as arising from either charge migration to protein surfaces freshly exposed due to unfolding, or the rearrangement (and cleavage of interfacial) salt bridges in the gas phase [14]. Our data is consistent with key aspects of both models: we observe unfolding of the dimers, and we see strong evidence for novel salt-bridge formation. However, our data is not explained fully by either model. Most crucial is the comparison between G37R at WT SOD1. We found that, due to forming an intra-monomer salt-bridge, the G37R dimer unfolded less, dissociated more asymmetrically, and produced a more compact 7+ monomer. This does not

fit the unfolding model, that would predict the attenuation of unfolding (and more compact monomer) of G37R to result in more symmetric dissociation. Nor does it readily fit the interfacial salt-bridge model, as the mutation and the new bond it forms lie away from the dimer interface. We have proposed here a mechanism that rationalises our data, using concepts from both models, and leveraging the understanding that has been developed about charge separation, location, and motion on gas-phase proteins[44, 47-48, 53].

Based on our work here, it is our hypothesis that 1) unfolding is a salient aspect of asymmetric dissociation, 2) that it happens in the context of new salt bridges being formed upon desolvation[14, 40, 42] and during activation, and 3) the associated charge migration[9] depends not just crudely on surface area[10-13] but on the specific residues and their local environment. We also think it very probable that 4) heterolytic cleavage of interfacial salt-bridges[14] plays an important role. This hypothesis places a lot of value on specific residues, and their local environment and interactions, which will vary from one protein complex to another. As such it provides a natural rationalisation for the variation and specificity observed for protein complex unfolding and dissociation in vacuum, and provides further support to the notion that recording and comparing these pathways may have considerable analytical value.

As a step towards doing so quantitatively, we have presented an Arrhenius-type framework for analysis which, despite assumptions implicit therein and together with other recently presented methodologies[59], represents a means for meaningful and direct comparison between proteins in terms of the barriers on the free energy landscape. This work therefore represents a step towards maximising the utility of information extracted from native MS experiments where the protein folding funnel is explored by deliberate gas phase activation[21].

We note, however, that results obtained from such an approach are inexorably tied to the model (i.e. the number and sequence of unfolding and dissociation events) that is chosen. In line with Occam's razor, we used the simplest model afforded by the data and, though the model produced seemingly sensible quantitative insights into the data, it is possible (indeed, likely) that there are complexities to the mechanism of SOD1 unfolding and dissociation to which our data is not sensitive, and hence we are unjustified in modelling. In this regard, recent developments in IM-MS technology that allow specific conformers can be activated individually such that specific dissociation channels can be interrogated hold great promise in increasing the information content of the gas-phase activation experiment [45]. Such experiments will add to the arsenal of experimental and analysis approaches that will ultimately combine to allow the exhaustive, quantitative dissection of native proteins through all levels of their structure, from non-covalent assembly to peptide fragments.

ASSOCIATED CONTENT

Supporting Information

The Supporting Information is available free of charge on the ACS Publications website.

Supplementary tables and figures (PDF)

AUTHOR INFORMATION

Corresponding Authors

*E-mail: jyerbury@uow.edu.au

*E-mail: justin.benesch@chem.ox.ac.uk

Author Contributions

LM performed experiments, analysed data, and wrote the initial manuscript. JAH performed experiments, analysed data, and edited the manuscript. SPF analysed data and edited the manuscript. JAA designed experiments, analysed data and edited the manuscript. CK performed experiments, analysed data, and edited the manuscript. JLPB designed experiments, analysed data and edited the manuscript. JJY designed experiments, analysed data and edited the manuscript.

Notes

The authors do not declare any competing financial interests

ACKNOWLEDGMENTS

- The authors would like to thank the MSURRF group at the University of Wollongong for access to mass spectrometers. We thank Professor Mikael Oliveberg (Stockholm

University, Sweden) for the initial expression plasmids used in this work, and Professor Jennifer L. Beck (University of Wollongong, Australia) and Dr Blagojce Jovcevski (University of Adelaide, Australia) for helpful discussions. LM was supported by a UOW matching scholarship. SPF acknowledges financial support from the UK EPRSC under grant number EP/R005974/1. JLPB thanks the Royal Society for a University Research Fellowship (UF120251). JJY is supported by an NHMRC Career Development Fellowship (1084144) and a Dementia Teams Grant (1095215). The authors would also like to acknowledge an ARC LIEF grant (LE0882289) for purchase of the Synapt G1 HDMS mass spectrometer used in this work.

References

1. Ben-Nissan, G.; Sharon, M., The application of ion-mobility mass spectrometry for structure/function investigation of protein complexes. *Current opinion in chemical biology* **2018,** *42*, 25-33.

2. Calabrese, A. N.; Radford, S. E., Mass spectrometry-enabled structural biology of membrane proteins. *Methods (San Diego, Calif.)* **2018,** *147*, 187-205.

3. Lanucara, F.; Holman, S. W.; Gray, C. J.; Eyers, C. E., The power of ion mobility-mass spectrometry for structural characterization and the study of conformational dynamics. *Nature chemistry* **2014,** *6* (4), 281-94.

4. Stuchfield, D.; Barran, P., Unique insights to intrinsically disordered proteins provided by ion mobility mass spectrometry. *Current opinion in chemical biology* **2018,** *42*, 177-185.

5. Liko, I.; Allison, T. M.; Hopper, J. T. S.; Robinson, C. V., Mass spectrometry guided structural biology. *Curr. Opin. Structl. Biol.* **2016,** *40*, 136-144.

6. Benesch, J. L., Collisional activation of protein complexes: picking up the pieces. *J. Am. Soc. Mass Spectrom.* **2009,** *20* (3), 341-8.

7. Li, J.; Lyu, W.; Rossetti, G.; Konijnenberg, A.; Natalello, A.; Ippoliti, E.; Orozco, M.; Sobott, F.; Grandori, R.; Carloni, P., Proton Dynamics in Protein Mass Spectrometry. *J Phys Chem Lett* **2017,** *8* (6), 1105-1112.

8. Wysocki, V. H.; Tsaprailis, G.; Smith, L. L.; Breci, L. A., Mobile and localized protons: a framework for understanding peptide dissociation. *J Mass Spectrom* **2000,** *35* (12), 1399-406.

9. Mistarz, U. H.; Chandler, S. A.; Brown, J. M.; Benesch, J. L. P.; Rand, K. D., Probing the Dissociation of Protein Complexes by Means of Gas-Phase H/D Exchange Mass Spectrometry. *J Am Soc Mass Spectrom* **2019,** *30* (1), 45-57.

10. Benesch, J. L. P.; Aquilina, J. A.; Ruotolo, B. T.; Sobott, F.; Robinson, C. V., Tandem Mass Spectrometry Reveals the Quaternary Organization of Macromolecular Assemblies. *Chem. & Biol.* **2006,** *13*, 597 - 605.

11. Popa, V.; Trecroce, D. A.; McAllister, R. G.; Konermann, L., Collision-Induced Dissociation of Electrosprayed Protein Complexes: An All-Atom Molecular Dynamics Model with Mobile Protons. *J. Phys. Chem. B* **2016,** *120* (23), 5114-5124.

12. Sinelnikov, I.; Kitova, E.; Klassen, J., Influence of Coulombic Repulsion on the Dissociation Pathways and Energetics of Multiprotein Complexes in the Gas Phase. *J. Am. Soc. Mass. Spectrom.* **2007,** *18* (4), 617-631.

13. Wanasundara, S.; Thachuk, M., Theoretical Investigations of the Dissociation of Charged Protein Complexes in the Gas Phase. *J. Am. Soc. Mass. Spectrom.* **2007,** *18* (12).

14. Loo, R. R.; Loo, J. A., Salt Bridge Rearrangement (SaBRe) Explains the Dissociation Behavior of Noncovalent Complexes. *J. Am. Soc. Mass Spectrom.* **2016,** *27* (6), 975-90.

15. Ruotolo, B. T.; Hyung, S. J.; Robinson, P. M.; Giles, K.; Bateman, R. H.; Robinson, C. V., Ion mobility-mass spectrometry reveals long-lived, unfolded intermediates in the dissociation of protein complexes. *Angew. Chem. Int. Ed. Engl.* **2007,** *46* (42), 8001-4.

16. Pagel, K.; Hyung, S. J.; Ruotolo, B. T.; Robinson, C. V., Alternate dissociation pathways identified in charge-reduced protein complex ions. *Anal. Chem.* **2010,** *82* (12), 5363-72.

17. Zhong, Y.; Han, L.; Ruotolo, B. T., Collisional and Coulombic Unfolding of Gas-Phase Proteins: High Correlation to Their Domain Structures in Solution. *Angew. Chem.* **2014,** *126* (35), 9363-9366.

18. Zhou, M.; Dagan, S.; Wysocki, V. H., Impact of charge state on gas-phase behaviors of noncovalent protein complexes in collision induced dissociation and surface induced dissociation. *Analyst* **2013,** *138* (5), 1353-1362.

19. Wanasundara, S. N.; Thachuk, M., Free energy barrier estimation for the dissociation of charged protein complexes in the gas phase. *The journal of physical chemistry. A* **2009,** *113* (16), 3814-21.

20. Eschweiler, J. D.; Kerr, R.; Rabuck-Gibbons, J.; Ruotolo, B. T., Sizing Up Protein–Ligand Complexes: The Rise of Structural Mass Spectrometry Approaches in the Pharmaceutical Sciences. *Annu. Rev. Anal. Chem.* **2017,** *10* (1), 25-44.

21. Chandler, S. A.; Benesch, J. L., Mass spectrometry beyond the native state. *Current opinion in chemical biology* **2017,** *42*, 130-137.

22. McCord, J. M.; Fridovich, I., Superoxide Dismutase. An Enzymic function for Erythrocuprein (Hemocuprein). *J. Biol. Chem.* **1969,** *244* (22), 6049-6055.

23. Doucette, P. A.; Whitson, L. J.; Cao, X.; Schirf, V.; Demeler, B.; Valentine, J. S.; Hansen, J. C.; Hart, P. J., Dissociation of Human Copper-Zinc Superoxide Dismutase Dimers using Chaotrope and Reductant: Insights into the Molecular Basis for Dimer Stability. *J Biol. Chem.* **2004,** *279* (52), 54558-54566.

24. McAlary, L.; Yerbury, J. J.; Aquilina, J. A., Glutathionylation potentiates benign superoxide dismutase 1 variants to the toxic forms associated with amyotrophic lateral sclerosis. *Sci. Rep.* **2013,** *3*, 3275.

25. Redler, R.; Wilcox, K. C.; Proctor, E.; Fee, L.; Caplow, M.; Dokholyan, N. V., Glutathionylation at Cys-111 Induces Dissocation of Wild Type and FALS Mutant SOD1 Dimers. *Biochemistry* **2011,** *50*, 7057-7066.

26. Khare, S. D.; Caplow, M.; Dokholyan, N. V., FALS Mutations in Cu, Zn Superoxide Dismutase Destabilize the Dimer and Increase Dimer Dissociation Propensity: A Large-scale Thermodynamic Analysis. *Amyloid* **2006,** *13* (4), 226-235.

27. Zhuang, X.; Liu, S.; Zhang, R.; Song, F.; Liu, Z.; Liu, S., Identification of Unfolding and Dissociation Pathways of Superoxide Dismutase in the Gas Phase by Ion-Mobility Separation and Tandem Mass Spectrometry. *Anal. Chem.* **2014,** *86*, 11599 - 11605.

28. Lindberg, M. J.; Tibell, L.; Oliveberg, M., Common Denominator of Cu/Zn Superoxide Dismutase Mutants Associated with Amyotrophic Lateral Sclerosis: Decreased Stability of the Apo State. *Proc. Natl. Acad. Sci. USA* **2002,** *99* (26), 16607-16612.

29. Harrison, J. A.; Aquilina, J. A., Insights into the subunit arrangement and diversity of paradoxin and taipoxin. *Toxicon : official journal of the International Society on Toxinology* **2016,** *112*, 45-50.

30. Kondrat, F. D.; Struwe, W. B.; Benesch, J. L., Native mass spectrometry: towards high-throughput structural proteomics. *Methods Mol. Biol.* **2015,** *1261*, 349-71.

31. Eschweiler, J. D.; Rabuck-Gibbons, J. N.; Tian, Y.; Ruotolo, B. T., CIUSuite: A Quantitative Analysis Package for Collision Induced Unfolding Measurements of Gas-Phase Protein Ions. *Anal. Chem.* **2015,** *87* (22), 11516-11522.

32. Harrison, J. A.; Kelso, C.; Pukala, T. L.; Beck, J. L., Conditions for Analysis of Native Protein Structures Using Uniform Field Drift Tube Ion Mobility Mass Spectrometry and Characterization of Stable Calibrants for TWIM-MS. *Journal of The American Society for Mass Spectrometry* **2019,** *30* (2), 256-267.

33. Ruotolo, B. T.; Benesch, J. L. P.; Sandercock, A. M.; Hyung, S.-J.; Robinson, C. V., Ion mobility–mass spectrometry analysis of large protein complexes. *Nature Protocols* **2008,** *3*, 1139.

34. Salbo, R.; Bush, M. F.; Naver, H.; Campuzano, I.; Robinson, C. V.; Pettersson, I.; Jørgensen, T. J. D.; Haselmann, K. F., Traveling-wave ion mobility mass spectrometry of protein complexes: accurate calibrated collision cross-sections of human insulin oligomers. *Rapid Communications in Mass Spectrometry* **2012,** *26* (10), 1181-1193.

35. Leinartaite, L.; Saraboji, K.; Nordlund, A.; Logan, D. T.; Oliveberg, M., Folding catalysis by transient coordination of Zn2+ to the Cu ligands of the ALS-associated enzyme Cu/Zn superoxide dismutase 1. *J Am Chem Soc* **2010,** *132* (38), 13495-504.

36. Strange, R. W.; Antonyuk, S. V.; Hough, M. A.; Doucette, P. A.; Valentine, J. S.; Hasnain, S. S., Variable metallation of human superoxide dismutase: atomic resolution crystal structures of Cu-Zn, Zn-Zn and as-isolated wild-type enzymes. *Journal of molecular biology* **2006,** *356* (5), 1152-62.

37. Marklund, E. G.; Degiacomi, M. T.; Robinson, C. V.; Baldwin, A. J.; Benesch, J. L., Collision cross sections for structural proteomics. *Structure (London, England : 1993)* **2015,** *23* (4), 791-9.

38. Li, J.; Begbie, A.; Boehm, B. J.; Button, A.; Whidborne, C.; Pouferis, Y.; Huang, D. M.; Pukala, T. L., Ion Mobility-Mass Spectrometry Reveals Details of Formation and Structure for

GAA·TCC DNA and RNA Triplexes. *Journal of The American Society for Mass Spectrometry* **2019,** *30* (1), 103-112.

39. Vékey, K., Internal Energy Effects in Mass Spectrometry. *J. Mass Spectrom.* **1996,** *31* (5), 445-463.

40. Breuker, K.; McLafferty, F. W., Stepwise evolution of protein native structure with electrospray into the gas phase, 10(-12) to 10(2) s. *Proc Natl Acad Sci U S A* **2008,** *105* (47), 18145-52.

41. Meyer, T.; de la Cruz, X.; Orozco, M., An atomistic view to the gas phase proteome. *Structure (London, England : 1993)* **2009,** *17* (1), 88-95.

42. van der Spoel, D.; Marklund, E. G.; Larsson, D. S.; Caleman, C., Proteins, lipids, and water in the gas phase. *Macromol Biosci* **2011,** *11* (1), 50-9.

43. Allison, T. M.; Landreh, M.; Benesch, J. L. P.; Robinson, C. V., Low Charge and Reduced Mobility of Membrane Protein Complexes Has Implications for Calibration of Collision Cross Section Measurements. *Anal Chem* **2016,** *88* (11), 5879-5884.

44. Marchese, R.; Grandori, R.; Carloni, P.; Raugei, S., On the zwitterionic nature of gas-phase peptides and protein ions. *PLOS Comput. Biol.* **2010,** *6* (5), e1000775-e1000775.

45. Eldrid, C.; Ujma, J.; Kalfas, S.; Tomczyk, N.; Giles, K.; Morris, M.; Thalassinos, K., Gas Phase Stability of Protein Ions in a Cyclic Ion Mobility Spectrometry Traveling Wave Device. *Anal Chem* **2019,** *91* (12), 7554-7561.

46. Wyttenbach, T.; Pierson, N. A.; Clemmer, D. E.; Bowers, M. T., Ion mobility analysis of molecular dynamics. *Annu Rev Phys Chem* **2014,** *65*, 175-96.

47. Bonner, J.; Lyon, Y. A.; Nellessen, C.; Julian, R. R., Photoelectron Transfer Dissociation Reveals Surprising Favorability of Zwitterionic States in Large Gaseous Peptides and Proteins. *Journal of the American Chemical Society* **2017,** *139* (30), 10286-10293.

48. Bakhtiari, M.; Konermann, L., Protein Ions Generated by Native Electrospray Ionization: Comparison of Gas Phase, Solution, and Crystal Structures. *J Phys Chem B* **2019,** *123* (8), 1784-1796.

49. Popa, V.; Trecroce, D. A.; McAllister, R. G.; Konermann, L., Collision-Induced Dissociation of Electrosprayed Protein Complexes: An All-Atom Molecular Dynamics Model with Mobile Protons. *J Phys Chem B* **2016,** *120* (23), 5114-24.

50. Hart, P. J.; Liu, H.; Pellegrini, M.; Nersissian, A. M.; Gralla, E. B.; Valentine, J. S.; Eisenberg, D., Subunit Asymmetry in the Three-Dimensional Structure of a Human CuZnSOD Mutant Found in Familial Amyotrophic Lateral Sclerosis. *Protein Sci.* **1998,** *7*, 545 - 555.

51. Jurchen, J. C.; Williams, E. R., Origin of asymmetric charge partitioning in the dissociation of gas-phase protein homodimers. *J. Am. Chem. Soc.* **2003,** *125* (9), 2817-2826.

52. Jurchen, J. C.; Garcia, D. E.; Williams, E. R., Further studies on the origins of asymmetric charge partitioning in protein homodimers. *J. Am. Soc. Mass Spectrom.* **2004,** *15* (10), 1408-1415.

53. Marchese, R.; Grandori, R.; Carloni, P.; Raugei, S., A computational model for protein ionization by electrospray based on gas-phase basicity. *J Am Soc Mass Spectrom* **2012,** *23* (11), 1903-10.

54. Antonyuk, S.; Elam, J. S.; Hough, M. A.; Strange, R. W.; Doucette, P. A.; Rodriguez, J. A.; Hayward, L. J.; Valentine, J. S.; Hart, P. J.; Hasnain, S. S., Structural consequences of the familial amyotrophic lateral sclerosis SOD1 mutant His46Arg. *Protein Sci.* **2005,** *14* (5), 1201-1213.

55. You, Z.; Cao, X.; Taylor, A. B.; Hart, P. J.; Levine, R. L., Characterization of a Covalent Polysulfane Bridge in Copper−Zinc Superoxide Dismutase. *Biochemistry* **2010,** *49* (6), 1191-1198.

56. Clemmer, D. E.; Russell, D. H.; Williams, E. R., Characterizing the Conformationome: Toward a Structural Understanding of the Proteome. *Acc. of Chem. Res.* **2017,** *50* (3), 556-560.

57. Eschweiler, J. D.; Kerr, R.; Rabuck-Gibbons, J.; Ruotolo, B. T., Sizing Up Protein-Ligand Complexes: The Rise of Structural Mass Spectrometry Approaches in the Pharmaceutical Sciences. *Annu. Rev. Anal. Chem.* **2017,** *10* (1), 25-44.

58. Dixit, S. M.; Polasky, D. A.; Ruotolo, B. T., Collision induced unfolding of isolated proteins in the gas phase: past, present, and future. *Current opinion in chemical biology* **2018,** *42*, 93-100.

59. Yefremova, Y.; Melder, F. T. I.; Danquah, B. D.; Opuni, K. F. M.; Koy, C.; Ehrens, A.; Frommholz, D.; Illges, H.; Koelbel, K.; Sobott, F.; Glocker, M. O., Apparent activation energies of protein–protein complex dissociation in the gas–phase determined by electrospray mass spectrometry. *Anal. Bioanal. Chem.* **2017,** *409* (28), 6549-6558.

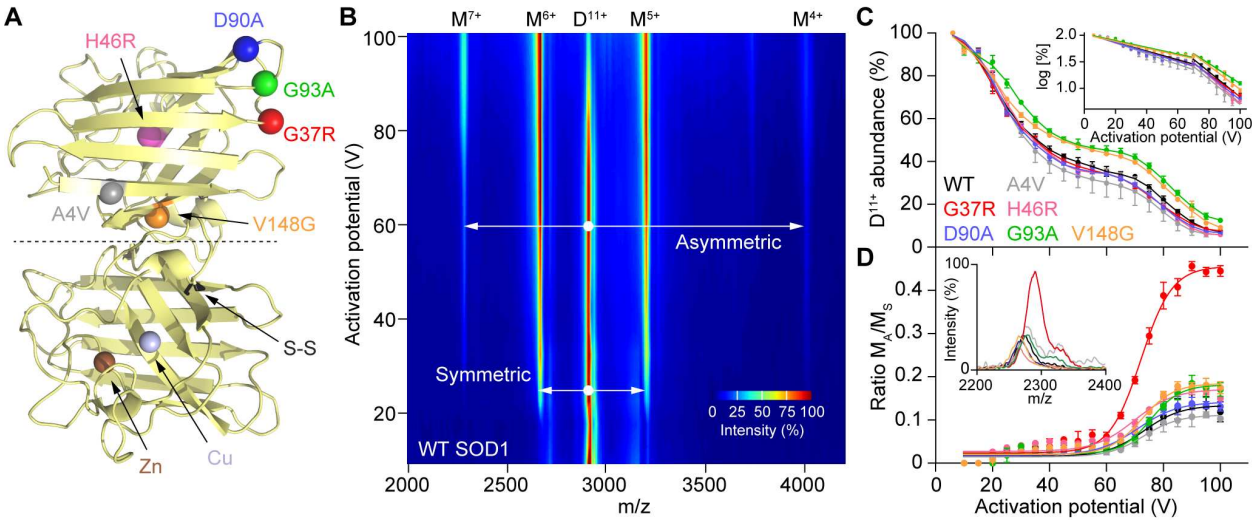

Figure 1. SOD1 dissociates into symmetric and asymmetric monomer populations. (A) Crystal structure of the native SOD1 dimer showing mutation locations as spheres on one monomer and the zinc, copper, and disulphide bond (S-S) on the other monomer. **(B)** Increasing activation potential (into the "trap" collision cell) applied to the SOD1-WT D^{11+} ion promotes dissociation into monomers with charge states ranging from 4+ to 7+. **(C)** Plotting the decrease in the relative abundance of the D^{11+} ion as a function of activation potential showed that the dissociation process was biphasic. This can be clearly seen in the log plot (inset). The addition of more phases (e.g. a triphasic fit) was not statistically justified by F-test, given the additional degrees of freedom. **(D)** The ratio of asymmetric (M_A) to symmetric (M_S) dissociation product abundances shows that G37R dissociated into asymmetric ions much more readily than other mutants, as can be seen in the abundance of the M^{7+} ion (inset, M^{7+} ion at 80 V compared to base peak). Error bars represent SD of the mean from 3 separate infusions of SOD1 protein.

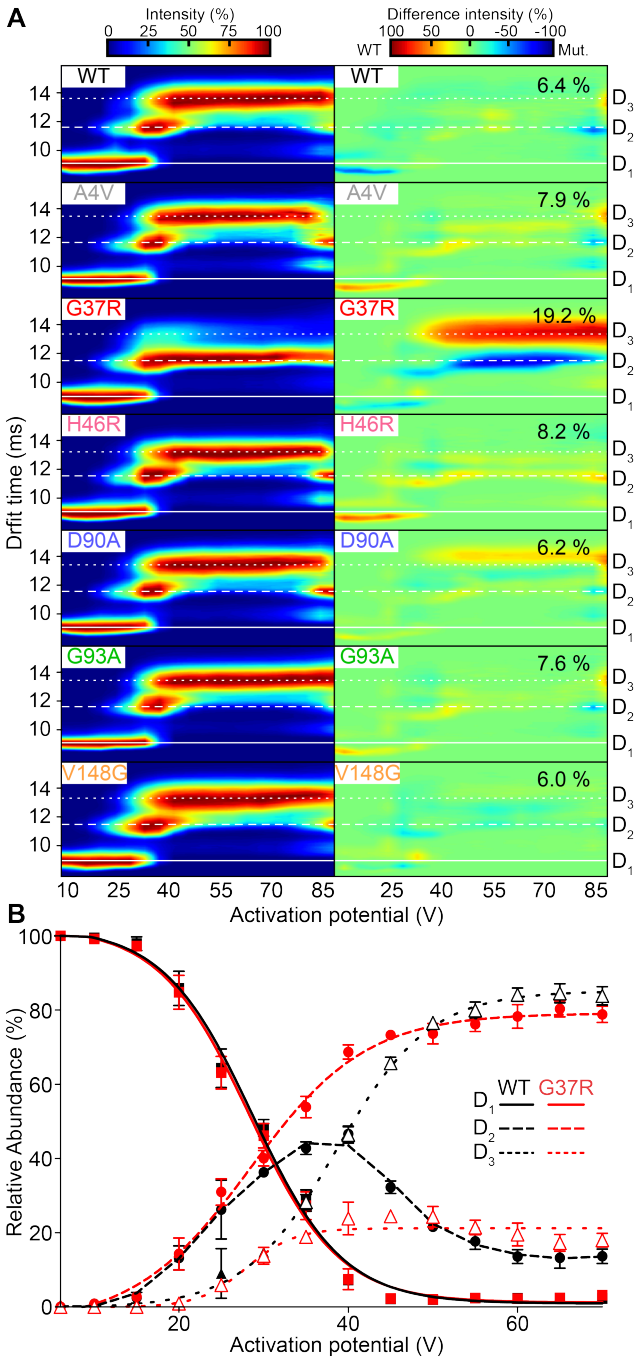

Figure 2. Unfolding of the SOD1 dimer proceeds via two transitions. (A) Left panels: CIU of SOD1 dimers (accelerated into the "trap" collision cell) showing the existence of two unfolding steps resulting in three conformers (D_1, D_2, D_3) for all proteins, with the exception of G37R which did not populate D_3 to a great extent (heat maps are normalized to the highest signal at each activation potential). Right panels: Comparing the WT to mutant data showed that the only mutant with significantly different CIU behaviour to WT was G37R (see Supplementary Fig. 3). Values correspond to RMSDs. **(B)** Plot of the relative abundances of each dimer state across activation energies reveals the persistence of G37R in D_2. D_1 squares, solid line; D_2 = open triangles, dotted line; D_3 circles, dotted line. Error bars represent SD of the mean from 3 separate infusions of SOD1 protein.

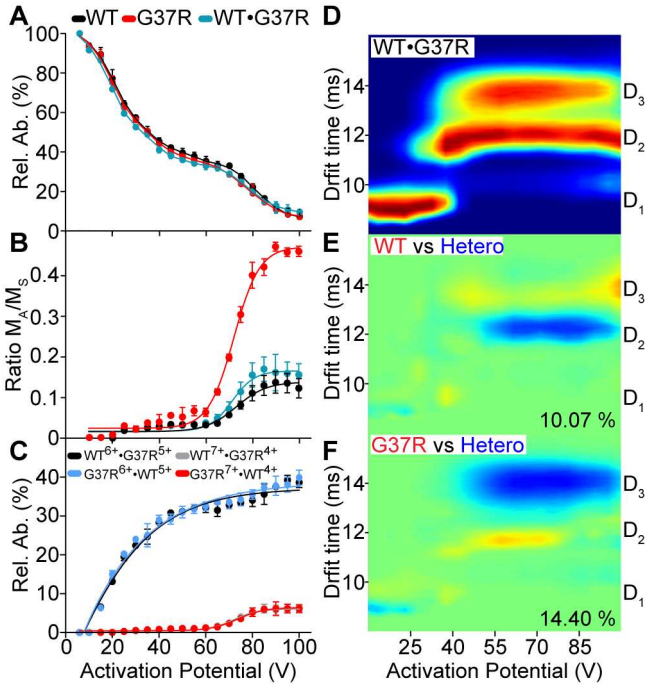

Figure 3. Dissociation and unfolding of a WT•G37R heterodimer. (A) Measurements of the relative abundance of dimer (circles), symmetric monomers (squares), and asymmetric monomers (triangles) of increasing activation potentials (into the "trap" collision cell) for WT (black), G37R (red) and heterodimer (turquoise). **(B)** Plot comparing the ratio of symmetric and asymmetric products for the homodimers and heterodimers. **(C)** Examination of the relative abundance of the products from the heterodimer shows no preference for either dissociation pathway (i.e. grey and red; and blue and black, are indistinguishable/overlap). **(D)** CIU fingerprint of the heterodimer. **(E)** Comparing the CIU fingerprint of WT homodimer to heterodimer. **(F)** Comparing the CIU fingerprint of G37R homodimer to heterodimer. Error bars represent SD of the mean from 3 replicate infusions of SOD1 protein.

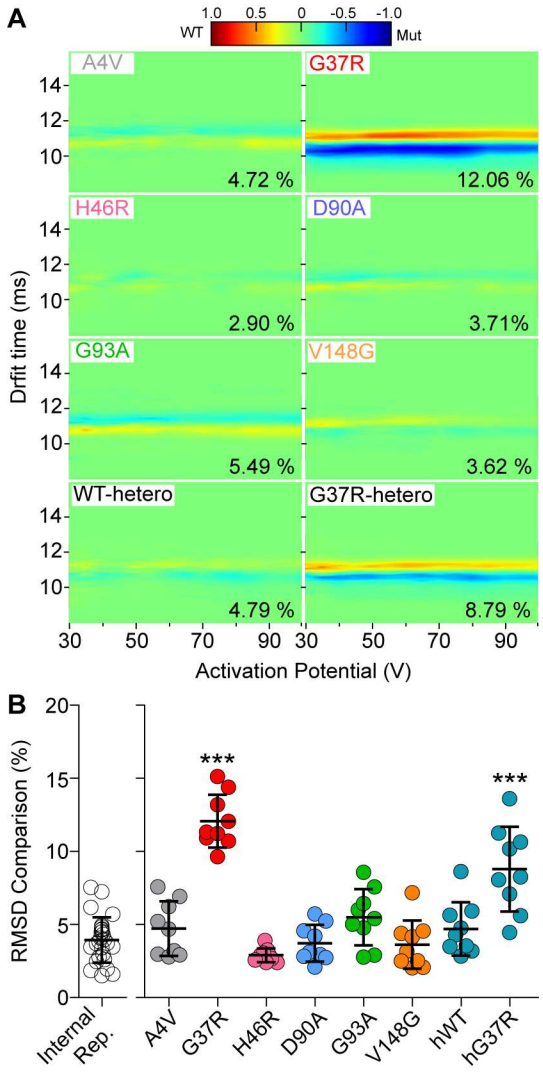

Figure 4. The G37R M^{7+} conformer is more compact than other SOD1 mutants. (A) CIU (acceleration into the "trap" collision cell) fingerprints comparing the dissociated M^{7+} conformer between WT and mutants where substantial differences are observed For G37R and heteroG37R. **(B)** RMSD comparison between each mutant's internal replicate monomer CIU fingerprints (Internal Rep. column) and each mutant monomer CIU replicate vs each monomer CIU replicate for the 7+ charge state. Significance was determined using Kruskal-Wallis analysis with Dunn's post-test comparing each column to the 'Internal Rep.' column. (*** = $p < 0.001$).

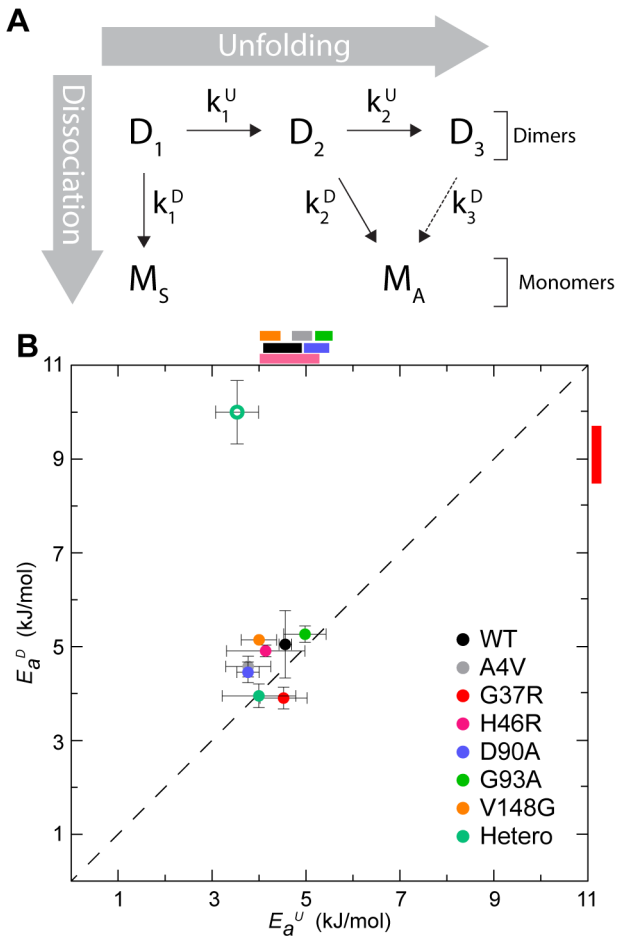

Figure 5. SOD1 dimer gas-phase dissociation and unfolding include thermal and athermal processes. (A) A model of SOD1 dimer gas-phase dissociation and unfolding as determined by the experimental data shown in this work. Briefly, upon activation the D_1 (dimer 1) either dissociates into symmetrically charged monomers (M_S) or unfolds into D_2 (dimer 2) which, upon further activation, dissociates into asymmetrically charged monomers (M_A) or unfolds into D_3 (dimer 3) which dissociates into M_A. **(B)** Plotting E_a^U against E_a^D for both the k_1^U-k_1^D juncture (closed circles) and the k_2^U-k_2^D juncture (open circles, and bars outside the plot) shows the relationship between the two processes for each mutant. Coloured bars outside the axis represent the standard error of the corresponding mutants for the axis they lie on and are shown this way since typically one of the processes at the k_2^U-k_2^D juncture is athermal. The WT•G37R heterodimer is the only dimer to have enough flux down both pathways (see R^2 values in supplementary table 1 and fits in supplementary figure 5). Error bars represent SD of the mean of at least 3 separate experiments. The dotted line represents $x = y$.

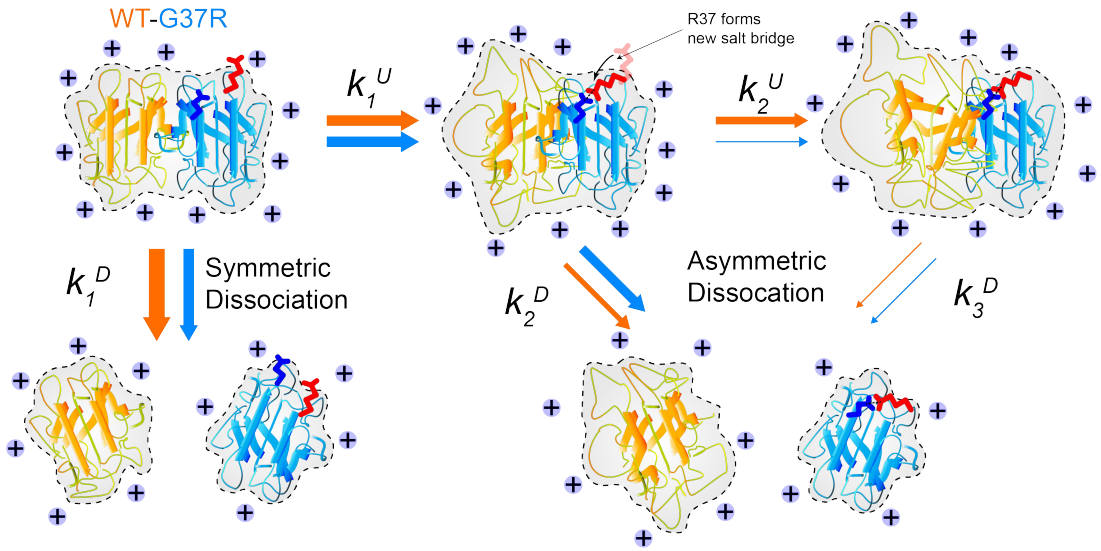

Figure 6. Schematic of a model of the dissociation and unfolding of a WT•G37R heterodimer. The initial dimer (D_1) contains WT (orange) and G37R (blue) monomers. At low activation potential D_1 dissociates (k_1^D) through the symmetric pathway to form M^{6+} and M^{5+} products. As the activation potential increases, D_1 unfolds (k_1^U) to the D_2 state where Arg37 forms a new salt-bridge. This leads to a greater tendency for the dimer to dissociate (k_2^D) at this stage, rather than unfolding further (k_2^U) to the D_3 state. In both the symmetric and asymmetric pathways, there is no preference for either the G37R or WT subunit to be preferentially charge enhanced/depleted (Fig. 3C). Arrow colour represents the propensity of dimer to proceed through a reaction for WT homodimers (orange) and G37R homodimers (blue).

Supporting Information

The trajectory taken by dimeric Cu/Zn superoxide dismutase through the protein unfolding and dissociation landscape is modulated by salt-bridge formation

Luke McAlary[†⊥], Julian A. Harrison[⊥], J. Andrew Aquilina[†⊥], Steven P. Fitzgerald[‡], Celine Kelso[⊥], Justin L.P. Benesch[§]* & Justin J. Yerbury[†⊥]*

[†]*Illawarra Health and Medical Research Institute, Wollongong, NSW 2522 Australia*

[⊥]*Molecular Horizons and School of Chemistry and Molecular Bioscience, Faculty of Science, Medicine and Health, University of Wollongong, NSW, Australia 2522*

[‡] *Department of Applied Mathematics, University of Leeds, Leeds, LS2 9JT, UK*

[§]*Department of Chemistry, Physical and Theoretical Chemistry Department, University of Oxford, Oxford, OX1 3QZ, UK*

* Address correspondence to justin.benesch@chem.ox.ac.uk and jyerbury@uow.edu.au

Abstract

The supporting information document here contains supplementary text, tables, and figures that relate to the manuscript titled "*The trajectory taken by dimeric Cu/Zn superoxide dismutase through the protein unfolding and dissociation landscape is modulated by salt-bridge formation*".

Supporting experimental section

Section 1.1

The rate equations describing the reaction model in Fig. 5A can be written in matrix form as

$$\frac{\mathrm{d}}{\mathrm{d}t}\begin{pmatrix} D_1 \\ D_2 \\ D_3 \end{pmatrix} = \begin{pmatrix} -k_1^D - k_1^U & 0 & 0 \\ k_1^U & -k_2^D - k_2^U & 0 \\ 0 & k_2^U & -k_3^U \end{pmatrix}\begin{pmatrix} D_1 \\ D_2 \\ D_3 \end{pmatrix},$$

and

$$\frac{\mathrm{d}}{\mathrm{d}t}\begin{pmatrix} M_\mathrm{A} \\ M_\mathrm{S} \end{pmatrix} = \begin{pmatrix} 0 & k_2^D & k_3^D \\ k_1^D & 0 & 0 \end{pmatrix}\begin{pmatrix} D_1 \\ D_2 \\ D_3 \end{pmatrix},$$

where D_1, D_2, D_3, M_A, and M_S denote, respectively, the relative concentrations of the states D_1, D_2, D_3, M_A, and M_S.

These can be solved analytically by diagonalization and, together with the initial conditions, determine the concentrations of the species as a function of the rates k_{ij} and measurement time, t. The resulting expressions are closed-form yet rather cumbersome, and are not reproduced here. The measured concentration for each species then leads to five equations in the five unknown rates k_{ij} (times t), which can be solved numerically for the rates at each activation potential. We did so, without employing any simplificaiton. Plotting the logarithm of the rates versus the reciprocal of the effective temperature (see next paragraph) reveals Arrhenius behaviour over a range of effective temperatures, $k_{ij}t = A\,t\,\exp\left(-E_{ij}/k_\mathrm{B}T_{eff}\right)$, and the activation energies can be fitted.

Supporting Information

Effective temperature can be calculated as follows using the method of Vékey[1]. The kinetic energy (E_k) of the ions is estimated to be given by $E_k = zeV$, were z is the integer charge on the protein, e the elementary charge, and V the accelerating potential into the collision cell. We next assume that all the kinetic energy is converted into internal modes in the collision cell: $E_{kin} = E_{int}$. The effective temperature, T_{eff}, can then be estimated using the equation $T_{eff} = E_{int}/(ckD)$, where k is Boltzmann's constant, D is the number of degrees of freedom in the protein (given by $3N$-6, where N is the number of atoms), and c is a temperature- and frequency-dependent factor, with a value of approximately 0.2 in organic molecules between 300 and 450 K[1].

Supporting tables and figures

Supplementary Table 1. R^2 values of the linear regression fits of the temperatures corresponding to each rate constant. Values in bold-face are those with $R^2 > 0.85$. Fits correspond to plots in Supplementary figure 5.

Rate constant	WT	A4V	G37R	H46R	D90A	G93A	V148G	Hetero
k_1^U	**0.97**	**0.92**	**0.96**	**0.92**	**0.93**	**0.97**	**0.96**	**0.93**
k_2^U	**0.96**	**0.93**	0.48	**0.95**	**0.98**	**0.97**	**0.96**	**0.91**
k_1^D	**0.92**	**0.98**	**0.86**	**0.94**	**0.98**	**0.92**	**0.88**	**0.93**
k_2^D	0.42	0.54	**0.88**	0.32	0.59	0.43	0.52	**0.88**
k_3^D	<0.1	<0.1	0.50	<0.1	<0.1	<0.1	<0.1	0.12

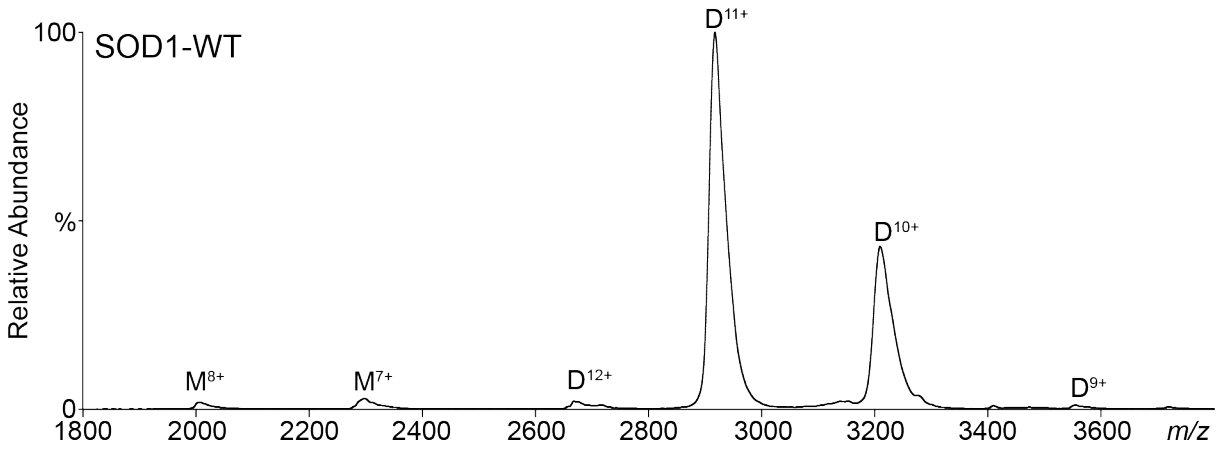

Supplementary Figure 1. Representative native mass spectrum of SOD1 WT. SOD1 WT was buffer exchanged into 200 mM NH_4OAc (pH 6.8) and nanoelectrosprayed under gentle conditions (10 μM monomeric concentration) which is composed of monomeric (M) and dimeric (D) forms of SOD1 WT. The charge states are marked in superscript.

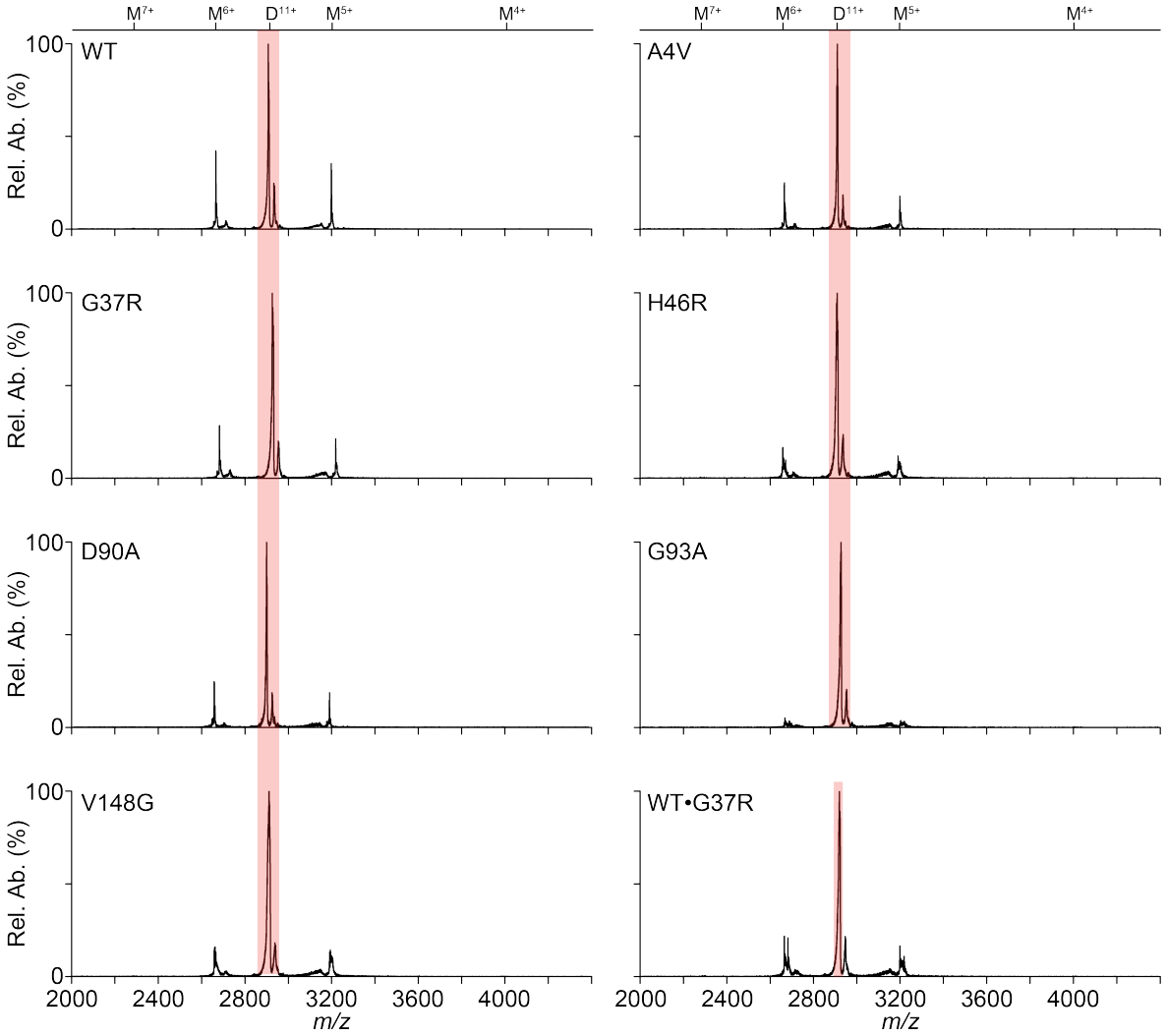

Supplementary Figure 2. MS/MS spectra of isolated SOD1 variant D^{11+} ions at low activation potential. MS/MS spectra of all SOD1 variant homodimers, and the WT•G37R heterodimer, at 20 V acceleration potential in the trap collision cell. The black bar above the spectra indicates the assignment of the peaks, and pink shading the m/z isolation window. Note at this low voltage, 6+ and 5+ monomer ions are readily observed, but 7+ and 4+ are not. Quantification of these peaks leads to the graphs show in Fig. 1C,D.

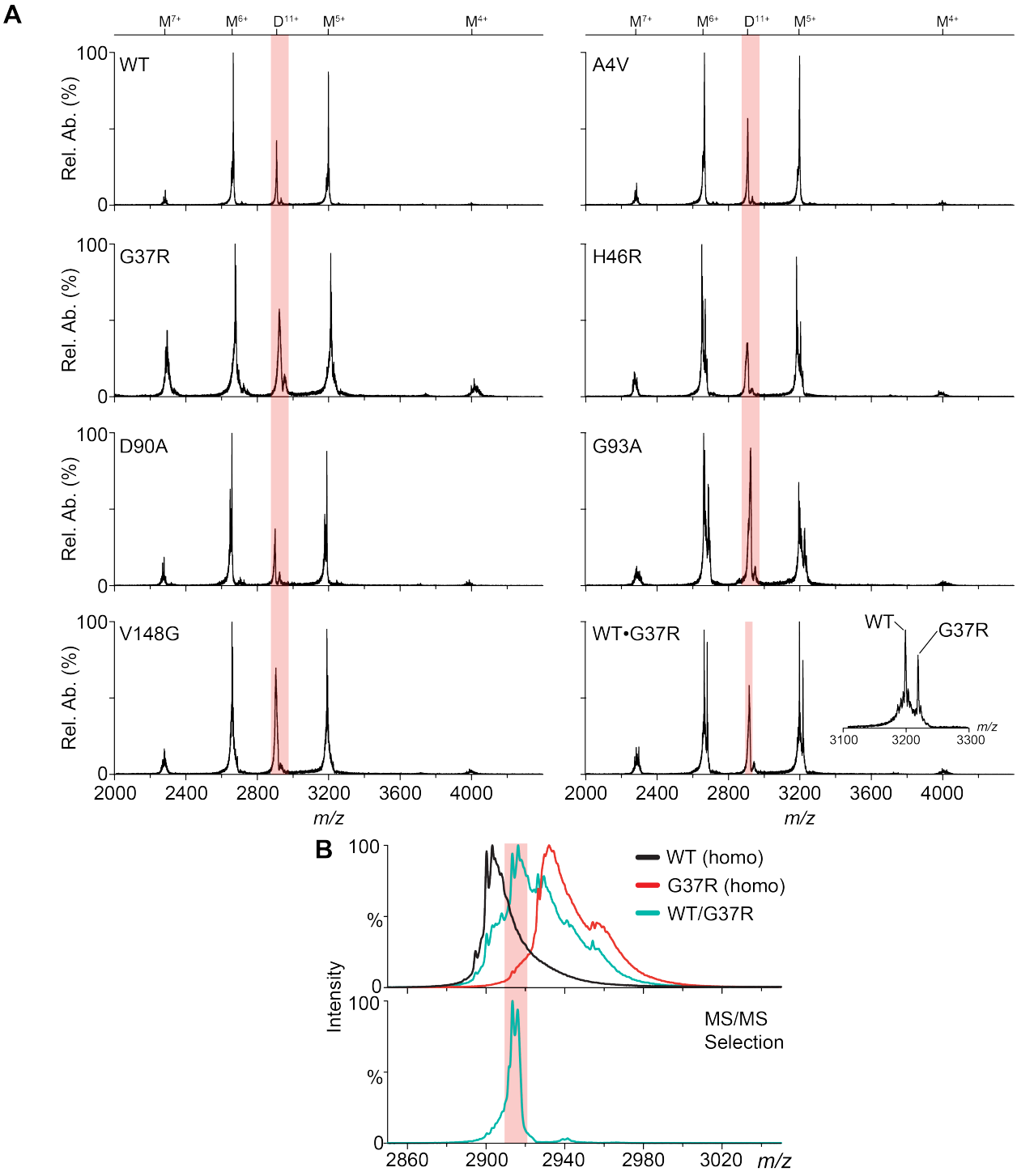

Supplementary Figure 3. (A) MS/MS spectra of all SOD1 variant homodimers, and the WT•G37R heterodimer, at 80 V acceleration potential in the trap collision cell. The black bar above the spectra indicates the assignment of the peaks, and pink shading the m/z isolation window. Inset in the WT•G37R heterodimer spectra is a spectra showing the M^{5+} ion in finer detail where both WT and G37R monomers are being produced. **(B)** Narrowing the isolation window (pink) centered at ~2910 *m/z*, it was possible to select 11+ precursors enriched for WT•G37R heterodimers. Black and red spectra are overlays of WT and G37R homodimers, respectively, from infusions separate to the heterodimer infusion (teal).

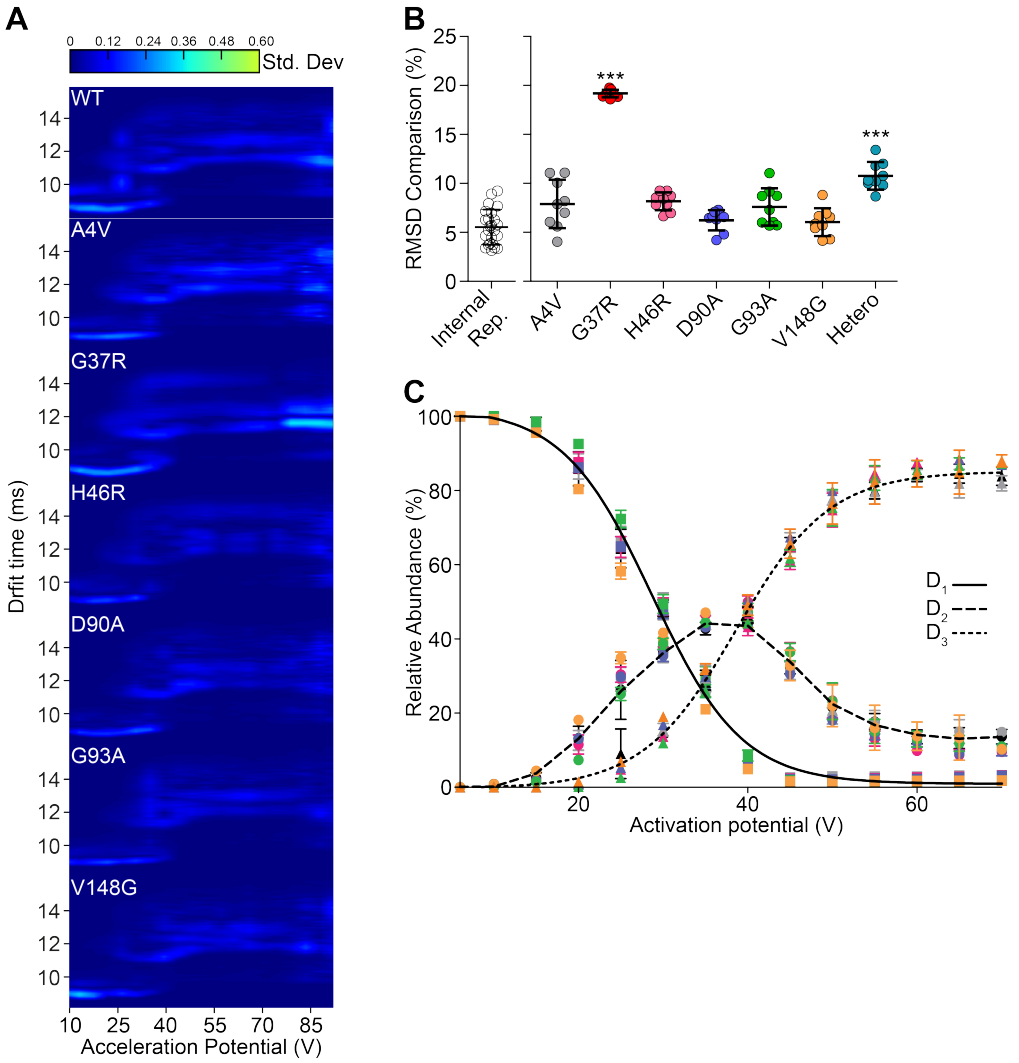

Supplementary Figure 4. (A) Standard deviation plots of CIU fingerprints of all SOD1 variants. **(B)** RMSD comparison between each mutant's internal replicate dimer^{11+} CIU fingerprints (Internal Rep. column) and each mutant dimer^{11+} CIU replicate *vs* each WT dimer^{11+} CIU replicate. **(C)** The relative abundances of the 3 different conformers (D_1, D_2, and D_3) of D^{11+} across activation potentials in the trap. Error bars represent SD of the mean from at least 3 separate infusions of protein. Significance was determined using Kruskal-Wallis analysis with Dunn's post-test comparing each column to the 'Internal Rep.' column (*** = $p < 0.001$).

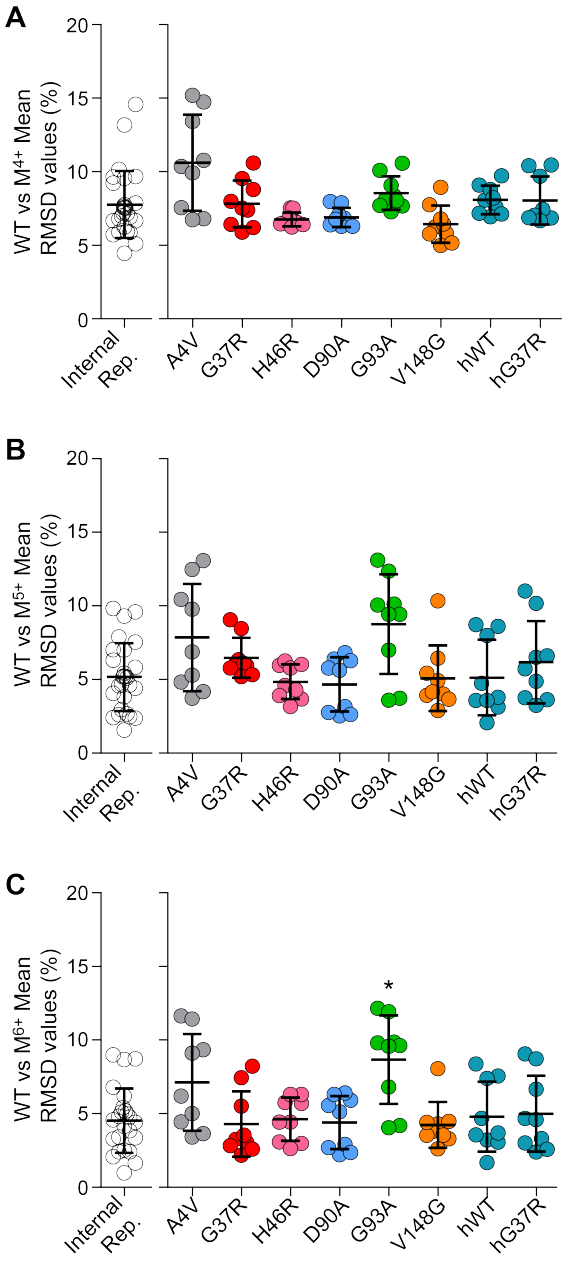

Supplementary Figure 5. RMSD comparison between each mutant's internal replicate monomer CIU fingerprints (Internal Rep. column) and each mutant monomer CIU replicate *vs* each monomer CIU replicate at the 4+ **(A)**, 5+ **(B)**, and 6+ **(C)** charge states. Significance was determined using Kruskal-Wallis analysis with Dunn's post-test comparing each column to the 'Internal Rep.' column. (* = $p < 0.05$).

Supplementary Table 2. Measurements of the CCS values for SOD1 WT monomers and dimers under different activation potentials.

		Ruotolo calibration[2]		Salbo calibration		X-ray[4]	Comparison[5]	*vs* X-ray[4]		Collision radius (Å)	
Species[1] (CE V)	*z*	CCS (Å^2)	RSD	CCS (Å^2)	RSD	CCS (Å^2)	Ruotolo/Salbo	Ruotolo	Salbo	IMPACT	Ruotolo
D (6 V)	10	2673	0.7	2675	0.7	2921	99.95	91.51	91.56	30.5	29.1
	11	2725	0.1	2726	0.1		99.93	93.27	93.33		29.4
	12	2814	0.4	2816	0.3		99.91	96.33	96.42		29.9
D CID (40 V)	11	3098	1.5	3127	1.5	2921	99.08	106.05	107.03	30.5	31.4
D CID (80 V)	11	3285	1.2	3283	1.0	2921	100.06	112.45	112.38	30.5	32.33
M CID (80 V)	7	1908	0.7	1903	0.9	1768	100.28	107.91	107.61	23.7	24.6
	6	1579	0.1	1571	0.5		100.52	89.33	88.88		22.4
	5	1464	0.5	1454	1.0		100.63	82.87	82.35		21.6
	4	1380	0.8	1370	1.4		100.72	78.19	77.63		21.0

[1] D = Dimer, M = Monomer, and CID = collision induced dissociation

[2] Calibrated using the method of Ruotolo, Benesch, Sandercock, Hyung and Robinson [2]

[3] Calibrated using the method of Salbo, Bush, Naver, Campuzano, Robinson, Pettersson, Jørgensen and Haselmann [3]

[4] Calculated from the crystal structure using IMPACT [4] with using previously reported radii [5]

[5] Calculated from $\frac{\text{Ruotolo CCS}}{\text{Salbo CCS}} \times 100$

[6] Calculated from $\frac{\text{Experimental CCS}}{\text{IMPACT CCS}} \times 100$

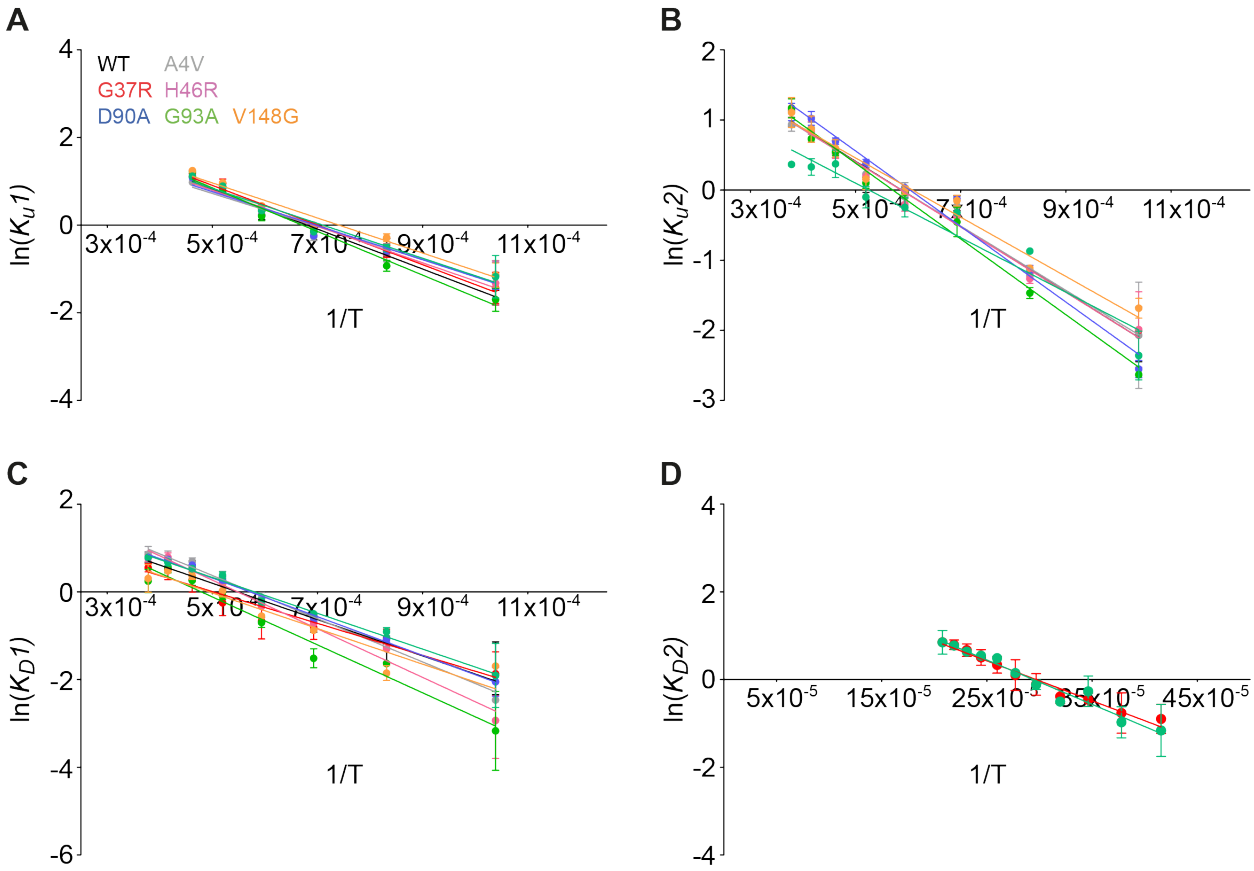

Supplementary Figure 6. (A) Linear regression fits of effective temperatures for k_1^U. **(B)** Linear regression fits of effective temperatures for k_2^U. **(C)** Linear regression fits of effective temperatures for k_1^D. **(D)** Linear regression fits of effective temperatures for k_2^D. Fits are shown only for those variants which had R values > 0.85 for any of the kinetic processes.

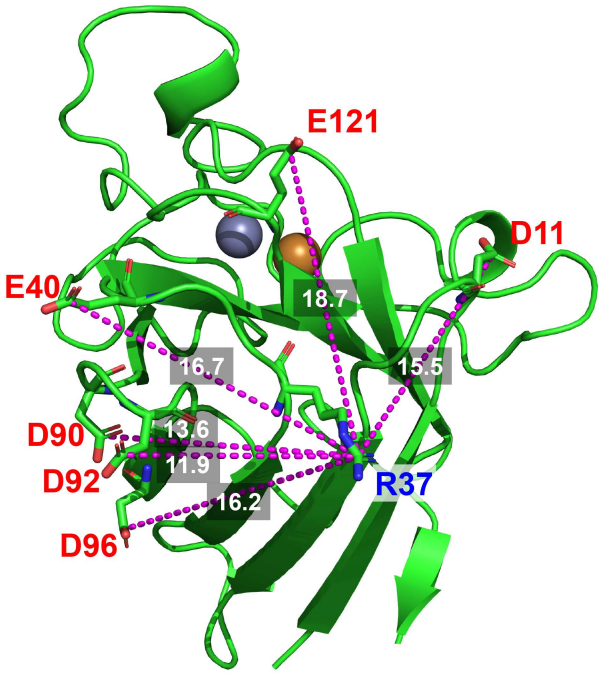

Supplementary Figure 7. Distance measurements of the closest Asp and Glu residues (red) to R37 (blue) in a SOD1 G37R x-ray crystal structure (PDB: 1AZV). Black labels indicate the angstrom (Å) distance from each residue to R37. The closest negatively charged residue is D92 at 11.9 Å, further than the minimum ~5 Å that is necessary for salt-bridge formation.

Supplementary Table 3a. Measured intra-monomer distances between R groups and alpha carbons of SOD1 G37R crystal structure (1AZV).

Amino Acid	Distance from R37 Cα (Å)	Distance from R37 R-group (Å)
D11	12.2	15.5
E40	9.0	16.7
D90	10.1	13.6
D92	7.7	11.9
D96	12.1	16.2
E121	11.8	18.7

Supplementary Table 3b. Measured inter-monomer distances between R groups and alpha carbons of SOD1 G37R crystal structure (1AZV).

Amino Acid	Distance from R37 Cα (Å)	Distance from R37 R-group (Å)
D11	22.0	24.3
D52	21.8	25.0

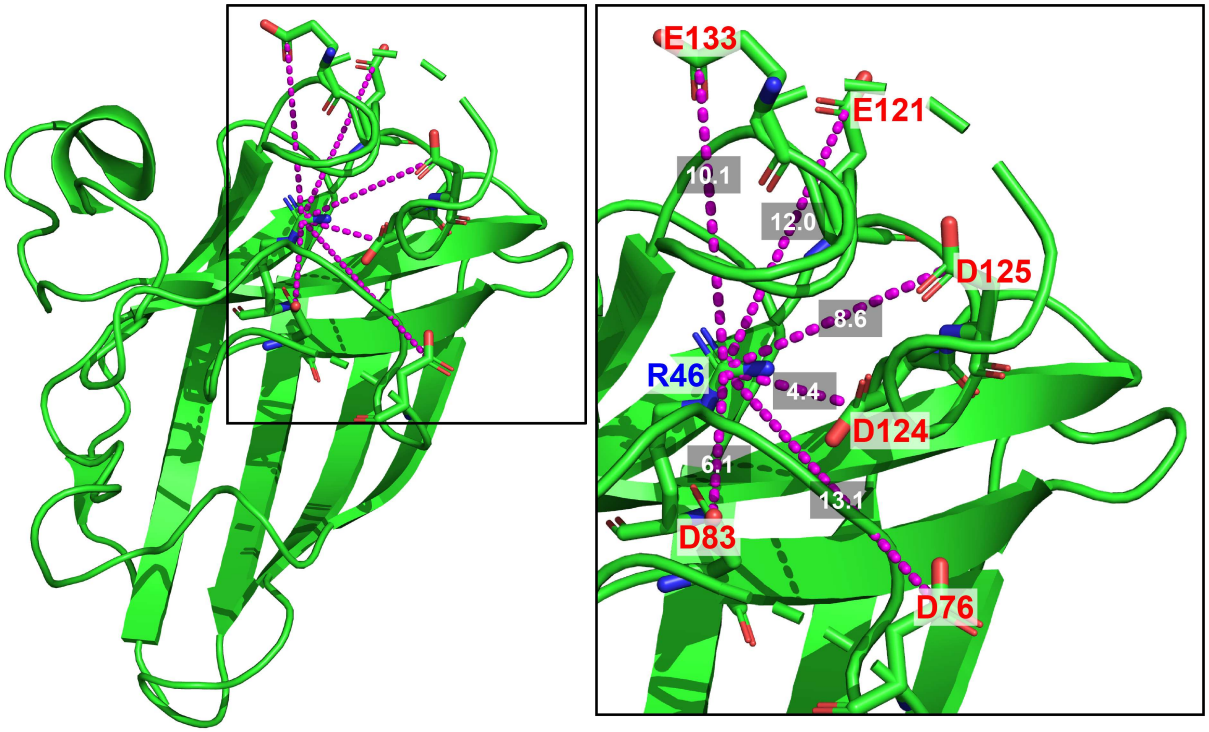

Supplementary Figure 8. Distance measurements of the closest Asp and Glu residues (red) to R46 (blue) in a SOD1-H46R x-ray crystal structure (PDB: 3K91). Black labels indicate the angstrom (Å) distance from each residue to R37. The closest negatively charged residue is D124 at 4.4 Å, less than the minimum ~5 Å that is necessary for salt-bridge formation.

Supplementary Table 4. Measured distances between R groups and alpha carbons of SOD1-H46R crystal structure (3K91).

Amino Acid	Distance from R46 Cα (Å)	Distance from R46 R-group (Å)
D76	13.9	13.1
D83	4.5	6.1
E121	11.8	12.0
D124	8.5	***4.4***
D125	11.5	8.6
E133	14.0	10.1

Supplementary References

(1) Vékey, K. *Journal of Mass Spectrometry* **1996**, *31*, 445.

(2) Ruotolo, B. T.; Benesch, J. L. P.; Sandercock, A. M.; Hyung, S.-J.; Robinson, C. V. *Nature Protocols* **2008**, *3*, 1139.

(3) Salbo, R.; Bush, M. F.; Naver, H.; Campuzano, I.; Robinson, C. V.; Pettersson, I.; Jørgensen, T. J. D.; Haselmann, K. F. *Rapid Communications in Mass Spectrometry* **2012**, *26*, 1181.

(4) Marklund, E. G.; Degiacomi, M. T.; Robinson, C. V.; Baldwin, A. J.; Benesch, J. L. *Structure (London, England : 1993)* **2015**, *23*, 791.

(5) Li, J.; Begbie, A.; Boehm, B. J.; Button, A.; Whidborne, C.; Pouferis, Y.; Huang, D. M.; Pukala, T. L. *Journal of The American Society for Mass Spectrometry* **2019**, *30*, 103.